Modelling oxygen (^{18}O, ^{17}O, ^{16}O) and hydrogen (^{2}H, ^{1}H) water isotopes in the coupled numerical climate model iLOVECLIM (version 1.1.5)

Thomas Extier[1], Thibaut Caley[1], Didier M. Roche[2,3]

[1] Univ. Bordeaux, CNRS, Bordeaux INP, EPOC, UMR 5805, F-33600 Pessac, France.

5 [2] Laboratoire des Sciences du Climat et de l'Environnement, LSCE/IPSL, CEA-CNRS-UVSQ, Université Paris-Saclay, 91191 Gif-sur-Yvette, France.

[3] Earth and Climate Cluster, Faculty of Sciences, Vrije Universiteit Amsterdam, De Boelelaan 1085, 101 HV Amsterdam.

Correspondence to: Thomas Extier (thomas.extier@u-bordeaux.fr)

Abstract.

10 Stable water isotopes are used to infer changes in the hydrological cycle for different climate periods in climatic archive and numerical climate models. Following previous developments of δ^{18}O in the intermediate complexity model iLOVECLIM, we present here the implementation of the δ^{2}H and δ^{17}O water isotopes in the different components of this coupled numerical climate model, and calculate the d-excess and ^{17}O-excess. Results of a 5,000 years equilibrium simulation under preindustrial conditions are analysed and compared to observations for the atmosphere and the ocean components.

15 In the atmospheric component, the model correctly reproduces the first order global distribution of the δ^{2}H and d-excess as observed in the data, even if local differences are observed. The latitudinal gradient is also correctly reproduced in our model and fits previous water isotopes enabled General Circulation Models simulations despite a simplified atmospheric component in iLOVECLIM. One exception is observed in Antarctica where the model does not correctly estimate the water isotope composition, consequence of the non-conservative behaviour of the advection scheme at very low moisture content. For the

20 ocean, the model also simulates adequate isotopic composition in comparison to the observations, except for local areas such as in the surface Arabian Sea, a part of the Arctic and West equatorial Indian ocean. Data-model evaluation also presents a good match for the δ^{2}H over the entire water column in the Atlantic Ocean, reflecting the influence of the different water masses. Modelled δ^{17}O and ^{17}O-excess are also evaluated against measurements for the two components of the model and compare to another General Circulation Model.

1 Introduction

Stable water isotopologues (δ^{2}H, δ^{17}O, δ^{18}O) are important tracers of the hydrological cycle and are measured in a large variety of archives to reconstruct climate variations. At first order, the δ^{2}H and δ^{18}O isotopic ratios of precipitation measured in ice core can be used as a proxy of past temperature at the drilling site (e.g. Johnsen et al., 1972; Lorius et al., 1979; Jouzel, 2003). However, as they present the same variations, and following observations at lower latitudes, we can derive a second-order

30 parameter called deuterium excess (d-excess) from the difference between the δ^{2}H and δ^{18}O. During evaporation, kinetic non-

equilibrium processes affect the relationship between oxygen and hydrogen isotopes and lead to a deviation from the global
Meteoric Water Line (MWL), which represents the linear relationship between $\delta^{18}O$ and δ^2H (Dansgaard, 1964; Craig, 1961):

$$d-\text{excess} = \delta^2H - 8 \times \delta^{18}O \tag{1}$$

35

This parameter can be used to provide additional constraints on past climates and changes in the atmospheric water cycle. The
deuterium excess is conventionally interpreted in terms of temperature at the moisture source or shifts in moisture origin
(Stenni et al., 2001; Vimeux et al., 2002; Masson-Delmotte et al., 2005) although precipitation, seasonality and moisture source
regions changes in the past can complicate its interpretation (Lewis et al., 2013; Landais et al., 2021). Another second-order

40 parameter can be derived from $\delta^{17}O$ measurements, the ^{17}O-excess (Landais et al., 2006), which is defined as:

$$^{17}O-\text{excess} = \ln\left(\frac{\delta^{17}O}{1000} + 1\right) - 0.528 \times \ln\left(\frac{\delta^{18}O}{1000} + 1\right) \tag{2}$$

The ^{17}O-excess is then multiplied by 10^6 and expressed in per meg since magnitudes are very small (Landais et al., 2008). Note

45 that we used the logarithm notation for ^{17}O-excess following Luz and Barkan (2005). The ^{17}O-excess is controlled by kinetic
fractionation during evaporation and is commonly used to give information on the relative humidity over the ocean (Landais
et al., 2008; Risi et al., 2010; Uemura et al., 2010).

Among the new proxies to document the water isotopic ratio in precipitation, the hydrogen isotope composition of plant lipids

50 wax (alkanes) has been found to reflect predominantly local continental rainfall fluctuations (e.g. Schefuß et al., 2005; Collins
et al., 2013; Kuechler et al., 2013). Isotopic changes are primarily controlled by moisture loss by evapotranspiration, soil waters
conditions and precipitations rates, but the vegetation and isotopic enrichment effects are also to consider (Hou et al., 2008;
Sachse et al., 2012; Kahmen et al., 2013a,b). A new method has also been developed to extract the fossil water (fluid inclusions)
of speleothem records (Vonhof et al., 2006; van Breukelen et al., 2008). With this water, it becomes possible to realize

55 hydrogen and oxygen stable isotope analyses of fossil precipitation waters and document the deuterium excess values in the
past, outside the limited region of ice core presence.
Similarly to continental records, the isotopologues in ocean surface waters track regional freshwater balance and then the
hydrological cycle (Craig and Gordon, 1965). Water isotopologues in seawater can therefore be used as a proxy for salinity
since surface freshwater exchanges are important in determining the variability of both variables. Seawater oxygen isotope

60 concentration preserved in carbonate from organisms such as foraminifera allows estimations of past regional and qualitative
changes in salinity and ocean circulation (Schmidt et al., 2007; Caley et al., 2011). More recently, it has been suggested that
combining seawater hydrogen isotopes (δ^2H obtained from alkenones or other biomarkers) with oxygen isotope ($\delta^{18}O$ obtained

from zooplankton calcite shells of foraminifera) could be a promising way to quantitatively estimate of salinity variability (Rohling, 2007; Legrande and Schmidt, 2011, Leduc et al., 2013; Caley and Roche, 2015).

65

With the emergence of new paleoproxy to document water isotopologues in atmospheric and oceanic components of the climate system, the necessity to develop and use isotope-enabled models, and in particular coupled ocean-atmosphere models, as never been greater (e.g. Risi et al., 2012; Werner et al., 2016; Cauquoin et al., 2019). These later allow more complex assumptions related to paleoclimatic proxies to be examined (LeGrande and Schmidt, 2006; Schmidt et al., 2007). For example,

70 simulation of climate and its associated isotopic signal can provide a "transfer function" between isotopic signal and the considered climate variable such as precipitation rate/water isotopes in precipitation or salinity/water isotopes in seawater relationships. Furthermore, the use of intermediate complexity model, given the computational time facility, allows to improve our understanding of the relationship between deuterium excess and climate over a broad range of simulated climate changes.

75 Oxygen isotopes (18, 16) have been implemented in the three-dimensional model of intermediate complexity iLOVECLIM, allowing fully coupled atmosphere-ocean simulations. The detailed implementations of oxygen isotopes (18, 16) in iLOVECLIM and the evaluation against observed data in water samples and carbonates can be found in Roche (2013), Roche and Caley (2013) and Caley and Roche (2013). In the present manuscript, we present the design and the validation of δ^2H, δ^{17}O water isotopes as well as deuterium excess and ^{17}O-excess in the coupled iLOVECLIM climate model for the atmospheric

80 and oceanic components. The agreements and differences from the direct comparison between modelling results under pre-industrial conditions and multiple datasets will be discussed to determine the potential and the interest of using iLOVECLIM for paleoclimatic studies.

2 Description of the water isotopic scheme in iLOVECLIM

2.1 Atmospheric component ECBilt

85 The iLOVECLIM model (version 1.1.5) is a derivative of the LOVECLIM-1.2 climate model extensively described in Goosse et al. (2010). It is composed of an atmospheric, oceanic, land surface and vegetation component. The atmospheric component ECBilt is a quasi-geostrophic model with a T21 spectral grid (resolution of 5.6° in latitude and longitude) with a complete description of the water cycle from evaporation, condensation to precipitation. It is subdivided in three vertical layers at 800, 500 and 200 hPa with the humidity contained only on the first layer, that corresponds to the troposphere, and representative of

90 the total humidity content of the atmosphere. The other two dry layers correspond to the stratosphere. Evaporative water fluxes are added to this humid layer and vertical advection is computed. Water fluxes crossing the limit between the humid and dry layers are rained out as convective rain. For specific humidity of the humid layer larger than 80 % (set as the saturation humidity at given temperature), the excess water is removed as large-scale precipitation. If large scale precipitation occurs with negative temperatures, excess precipitation is removed as large-scale snowfall.

95

With regards to water isotopes, the main development lies in the atmospheric component in which evaporation, condensation and the existence of different phases (liquid and solid) all affect the isotopic conditions of the water isotopes. The methodology used to trace the hydrogen water isotopes in ECBilt is identical to the description made in Roche (2013) for the oxygen water isotopes. We used the same equations presented for the ^{18}O in Roche (2013) but with adapted fractionation coefficients for the

100   hydrogen and for ^{17}O. We present in this section the equations for $^{1}H^{2}H^{16}O / {}^{1}H_2{}^{16}O$. Equations are similar for $^{1}H_2{}^{17}O / {}^{1}H_2{}^{16}O$, but with different ratio and coefficient values. Additional information on general water scheme formulation can be found in Roche (2013).

In ECBilt, the water isotopic quantity is expressed as a single tracer of water similarly to Merlivat and Jouzel (1979). For $^{1}H^{2}H^{16}O / {}^{1}H_2{}^{16}O$, it is defined as a function of the quantity of precipitable water for the whole atmospheric column ($\tilde{q}$ which

105   depends on the mass of the water, the surface area of the cell and the water density) and of the ratio (R^H) between the number of moles of $^{1}H^{2}H^{16}O$ and the number of moles of $^{1}H_2{}^{16}O$:

$$\tilde{q}^H = \tilde{q} \times R^H \tag{3}$$

110   The isotopic composition then changes within the water cycle, from evaporation to precipitation. The evaporation term for hydrogen water isotopes cannot be simply written like for the humidity because there is no vertical discretization for water isotopes in the model. A solution is to compute the water isotopic ratio in the evaporation following adapted formulations from Cappa et al. (2003) and Roche (2013). The hydrogen isotopic ratio of evaporating moisture can then be written as:

115    $$R_E^H = \alpha_{diff}^* \left(\frac{R_{eq}^H - h_a^* R_a^H}{1 - h_a^*} \right) \tag{4}$$

where $R^H{}_{eq}$ is the isotopic ratio at equilibrium with the ocean, $R^H{}_a$ the isotopic ratio in the free atmosphere and $h^*{}_a$ is an apparent relative humidity factor for the free atmosphere. $\alpha^*{}_{diff}$ is a ratio of molecular diffusivity and defined for the hydrogen such as:

120    $$\alpha_{diff}^* = \left(\frac{D^H}{D} \right)^n \tag{5}$$

with D^H the molecular diffusivity of water $^{1}H^{2}H^{16}O$, D the molecular diffusivity of water $^{1}H_2{}^{16}O$ and n a coefficient that varies with turbulence and evaporative surface (Brutsaert, 1975; Mathieu and Bariac, 1996). The molecular diffusivity ratio for $^{1}H^{2}H^{16}O / {}^{1}H_2{}^{16}O$ is set to 0.9755 (Merlivat, 1978) and 0.9855 for $^{1}H_2{}^{17}O / {}^{1}H_2{}^{16}O$ (Barkan and Luz, 2007).

125

Since ECBilt only includes three layers, it is supposed that precipitation always forms in isotopic equilibrium with the surrounding moisture with instantaneous rainout to the surface. The precipitations (convective and large scale) and snow are in equilibrium with isotopic values at tropopause, mid-troposphere and tropopause respectively. When computing the precipitation and snow fractionation schemes (see Roche, 2013), we take into account the temperature, the fractionation

130 coefficients between the different water phases for the hydrogen, an enhanced kinetic fractionation at high latitude (Merlivat and Jouzel, 1979) and the ratio of hydrogen isotopes in vapor. In these equations, the hydrogen fractionation coefficient between liquid water and vapor is taken from Majoube (1971a) and depends on the temperature:

$$\alpha_{l-v}^H = \exp\left(\frac{24844}{T^2} - \frac{76.248}{T} + 0.052612\right) \tag{6}$$

135

For ^{17}O, the fractionation between liquid water and vapor is calculated from Majoube (1971a), Barkan and Luz (2005) and Barkan and Luz (2007):

$$\alpha_{l-v}^O = \exp\left(\frac{1137}{T^2} - \frac{0.4156}{T} - 0.0020667\right) \times 0.529 \tag{7}$$

140

The equilibrium fractionation coefficient between solid water and water vapor for hydrogen is taken from Merlivat and Nief (1967) and depend on the temperature as well:

$$\alpha_{s-v}^H = \exp\left(\frac{16289}{T^2} - 0.0945\right) \tag{8}$$

145

For ^{17}O, the fractionation between solid water and vapor is calculated from Majoube (1971b), Barkan and Luz (2005) and Barkan and Luz (2007):

$$\alpha_{s-v}^O = \exp\left(\frac{11.839}{T^2} - 0.028224\right) \times 0.528 \tag{9}$$

150

2.2 Ocean and land surface components

The oceanic component CLIO has a 3x3° horizontal resolution, 20 vertical layers and a free surface. In the ocean, the water isotopes are mass conserving and act as passive tracers under equilibrium fractionation ignoring the small fractionation implied by the presence of sea-ice (Craig and Gordon, 1965).

155 For the land surface model, the isotopes water implementation in the bucket follows the same procedure as for the water, except that equilibrium fractionation is assumed during phase changes. The ratio of hydrogen isotopes re-evaporation (R^H_{revap})

depends on the ratio of hydrogen isotopes of the land surface ($R^H_{landsurf}$) and on the equilibrium fractionation coefficient between liquid water and water vapor for hydrogen ($\alpha^H_{l\text{-}v}$) as a function of local surface temperature:

160 $$R^H_{revap} = \frac{R^H_{landsurf}}{\alpha^H_{l-v}} \qquad (10)$$

In the same way, evapotranspiration occurs from the soil bucket water with fractionation. A snow layer is also taken into account. Above a given threshold, the isotopic water and snow contents in the soil and snow buckets are routed to the ocean without fractionation.

2.3 Simulation setup

We present results of a 5,000 years equilibrium run under fixed pre-industrial boundary conditions. The atmospheric pCO_2 is chosen to be 280 ppm, methane concentration is 760 ppb and nitrous oxide concentration is 270 ppb. The orbital configuration is calculated from Berger (1978) with constant year 1950. We use present-day land sea mask, freshwater routing and interactive vegetation. With regards to the water isotopes, the atmospheric moisture is initialized at 0 and the δ^2H at 0 ‰. The consistency of our integration is checked by ensuring that the water isotopes are fully conserved in our coupled system. The model has been run at T21 spatial resolution (5.6° in longitude and latitude) and the output are computed with an annual timestep.

To investigate the seasonal variations of the model in comparison to the observations, and to estimate the range/dispersion of the modelled results, we performed a 100 years simulation starting from the equilibrium run, with monthly outputs for the climate and the isotopes.

2.4 Observational data

To allow for comparison and discussion with iLOVECLIM results, global hydrogen and d-excess isotopic datasets for the atmosphere (IAEA, 2006 and Masson-Delmotte et al., 2008) have been used. The original Global Network of Isotopes in Precipitation (GNIP) dataset (IAEA, 2006) has been subsampled to keep only the stations where the isotopic composition has been reported for a minimum of 3 calendar years within the period 1961-2008. To evaluate the seasonal evolution of the model, we looked at the evolution of precipitations and atmospheric isotopic composition at several locations distributed on multiple continents: Pretoria (25.73°S, 28.18°E), Belem (1.43°S, 48.48°W), Ankara (39.95°N, 32.88°E) and Reykjavik (64.13°N, 21.92°W). Present day measurements of $\delta^{17}O$ of precipitation and ^{17}O-excess from multiple studies (Vimeux et al., 2005; Landais et al., 2008, 2010, 2012; Risi et al., 2008; Luz and Barkan, 2010; Winkler et al., 2012; Tian et al., 2021) have also been used.

The GISS global seawater isotope database (Schmidt et al., 1999) has been used to compare the δ^2H and d-excess with the ocean component in the model.

3 Results and discussion

3.1 Water isotopic composition in the atmosphere

3.1.1 Annual $\delta^2 H_{precipitation}$

190 The annual mean modelled distribution of $\delta^2 H_{precipitation}$ is presented in comparison to observations from the GNIP database (IAEA, 2006) and from Masson-Delmotte et al. (2008) data over Antarctica on Fig. 1a. The latitudinal gradient from the poles to the equator is correctly reproduce in the model with depleted values at high latitudes (cold and dry regions) and enriched values at lower latitudes. Differences with the observations are however observed for specific regions. In central Africa and northern region of South America, the model underestimates the $\delta^2 H_{precipitation}$, which has higher values in the few measurements

195 available. This could be due to one of the well-known iLOVECLIM biases that is the overestimation of the precipitation in these regions. The west coast of South America also presents discrepancies between the model and the GNIP data (Fig. 1a). This could be related to the coarse model resolution that may not perfectly reproduce the observed $\delta^2 H_{precipitation}$ since the value is representative of a larger area. Finally, the modelled $\delta^2 H_{precipitation}$ over northern America and Europe is higher than the observations. The difference in atmospheric isotopic composition of precipitation over land and ocean is however well

200 reproduced in the model with high closed to zero values over the Pacific, Atlantic and Indian oceans and depleted values lower than -50 ‰ and -80 ‰ respectively over the Arctic and Austral oceans (Fig. 1a).

In order to further evaluate our model results, we compare a zonal transect with water isotopes enabled GCMs (General Circulation Models) results: ECHAM5 (Werner et al., 2011; Steiger et al., 2017), GISS (Schmidt et al., 2007), LMDZ4 (Risi

205 et al., 2012), MIROC (Kurita et al., 2011) and CAM (Lee et al., 2007). iLOVECLIM reproduces well the mean $\delta^2 H_{precipitation}$ for most latitudes, even if discrepancies are locally observed as well as strong depletions over Antarctica. From mid to low latitudes, iLOVECLIM shows similar mean $\delta^2 H_{precipitation}$ than other GCMs, with consistent values in comparison to the GNIP data (Fig. 2). At high latitudes of the northern hemisphere, iLOVECLIM shows a small decrease of $\delta^2 H_{precipitation}$ as observed in the other models and stays in the higher range of the observed $\delta^2 H_{precipitation}$. Our model also seems to better reproduce the

210 isotopic change above 80°N than in the other models. However, for latitudes below 65°S, the decrease of $\delta^2 H_{precipitation}$ in iLOVECLIM is lower than the one observed in ECHAM5, GISS, LMDZ4, MIROC and CAM models, as well as in the GNIP data with values between -149 and -453 ‰. These very low measured values over Antarctica can be explained by the low temperature (with a continental effect) and by other influences like moisture transport or the distance from the coast that add complexity in modelling this region (Fig. 2). Since iLOVECLIM only have three vertical layers in comparison to the 19 to 26

215 vertical layers for the other GCMs, we cannot properly reproduce the isotopic variations at these latitudes.
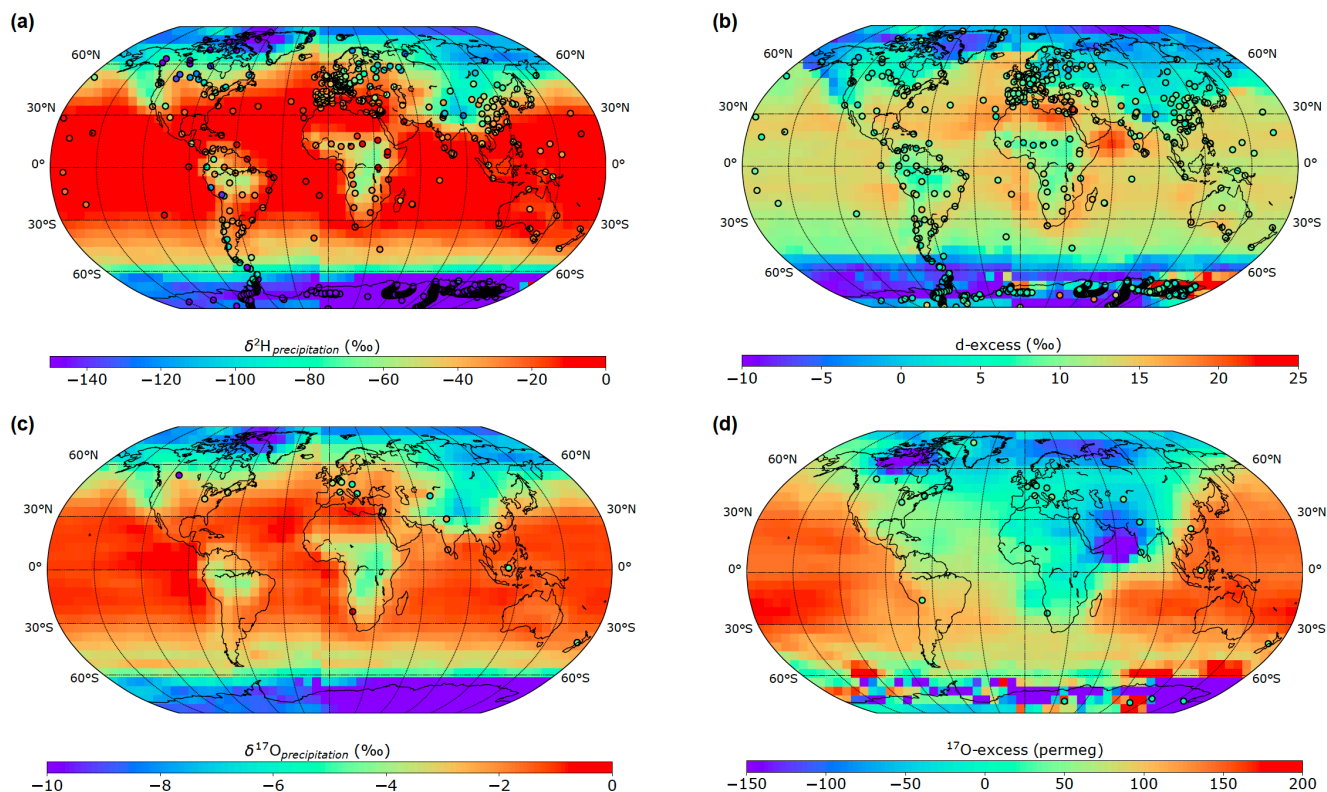
Figure 1: Model-data evaluation of the annual mean isotope distributions. (a) δ^2H in precipitation in iLOVECLIM compared to the Masson-Delmotte et al. (2008) and GNIP (IAEA, 2006) databases. (b) d-excess in iLOVECLIM compared to the Masson-Delmotte et al. (2008) and GNIP (IAEA, 2006) databases. (c) δ^{17}O in precipitation in iLOVECLIM compared to Luz and Barkan (2010) and Tian et al. (2021) datasets. (d) ^{17}O-excess in iLOVECLIM compared to Vimeux et al. (2005), Landais et al. (2008; 2010; 2012), Risi et al. (2008), Luz and Barkan (2010), Winkler et al. (2012) and Tian et al. (2021) datasets.

The linear relationship between δ^{18}O and δ^2H (δ^2H = 8*δ^{18}O + 10) established by Craig (1961) and defined as the global Meteorological Water Line can also be verified in the model. Figure 3 presents the relationship between the two isotopic compositions obtained with iLOVECLIM in comparison to the GNIP and Masson-Delmotte et al. (2008) databases. The model values match the GNIP observations and correctly reproduces the linear trend between the δ^{18}O and δ^2H of precipitation with values of the regression line similar to those of the GNIP data and close to the global Meteorological Water Line (Fig. 3). The correlation coefficient of the modelled isotopic results is very good with 0.99. The lowest modelled isotopic values are however not as depleted as these obtained from Masson-Delmotte et al. (2008) (up to -453 ‰ δ^2H vs -213 ‰ in the model) since the modelling of the isotopic composition over Antarctica depends on complex processes that are not well represented in the model. Figure 3 is then presented within the range of the modelled values (excluding some Antarctic values).
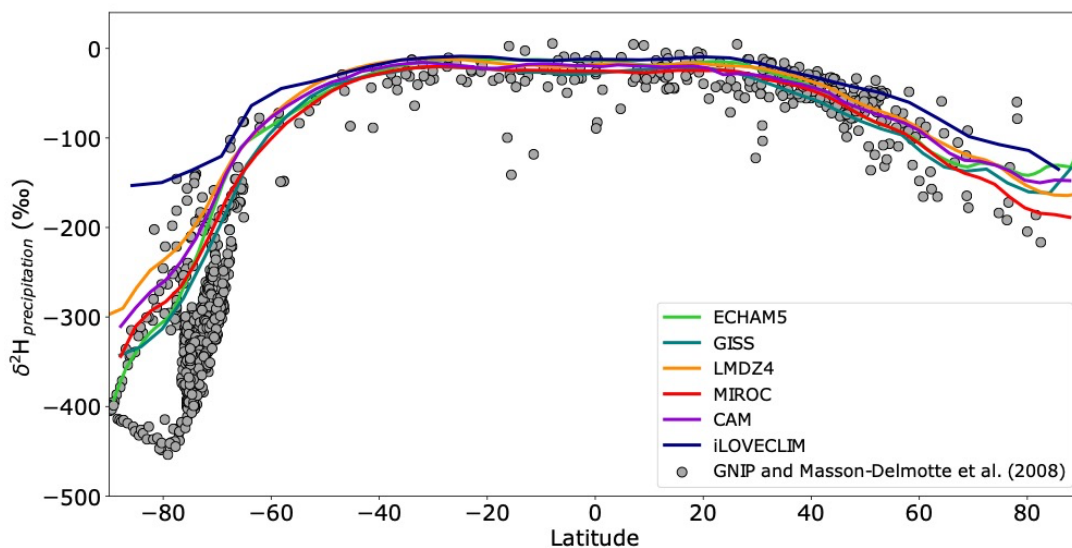
Figure 2: Zonal mean δ²H in precipitation in iLOVECLIM compared to several water-isotopes enabled GCMs: ECHAM5 (Steiger et al., 2018), GISS (Schmidt et al., 2007), LMDZ4 (Risi et al., 2012), MIROC (Kurita et al., 2011) and CAM (Lee et al., 2007). The GNIP (IAEA, 2006) and Masson-Delmotte et al. (2008) databases are also shown with the grey points.
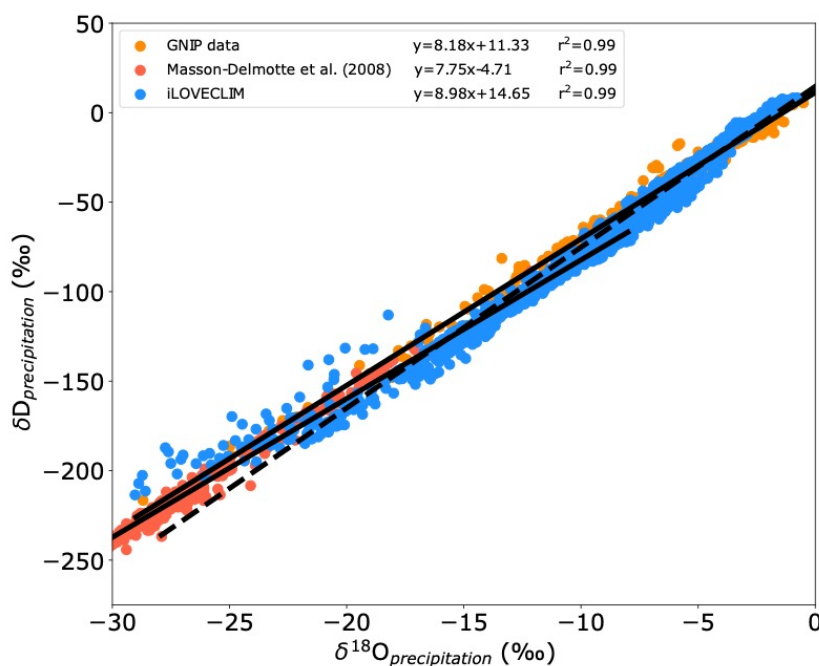
Figure 3: The global Meteorological Water Line as simulated in iLOVECLIM (in blue) compared to GNIP (IAEA, 2006) and Masson-Delmotte et al. (2008) data (in orange and red respectively). Regression lines are shown with a solid black line for the two datasets and with a dashed black line for the model.

3.1.2 Annual deuterium excess

245 The mean annual d-excess distribution is derived from the oxygen and hydrogen isotopic composition and presented in Fig. 1b. To evaluate the accuracy of the model, we compare the results to the GNIP (IAEA, 2006) and Masson-Delmotte et al. (2008) databases. As observed for the $\delta^2 H_{precipitation}$, the d-excess presents a latitudinal gradient with depleted negative values to the poles and enriched positive values to the equator (Fig. 1b). The modelled values fit well with the observations at global scale. Differences between the model and the observations remain for some regions like over India where the modelled d-

250 excess is slightly higher than the observations. The d-excess over Greenland, and especially the coastal areas, is negative whereas the few data points indicate positive values that are up to 20 ‰ higher. Similarly to the annual $\delta^2 H_{precipitation}$ distribution, the d-excess over Antarctica is not correctly reproduced in the model. The local data show values between 5 and 10 ‰ whereas the model calculates mostly negative d-excess, with values ranging from -10 to 10 ‰ and up to 25 ‰ or higher in the region of Adélie Land (Fig. 1b). Over the ocean, few d-excess data points are available but the model presents an overall good

255 agreement with the GNIP data with mean values ranging from -10 ‰ over the Arctic and Austal oceans to 17 ‰ over the Atlantic and Pacific oceans. A maximum in d-excess is reach over the Arabian sea with 20.6 ‰.

The relationship between the d-excess and the $\delta^2 H_{precipitation}$ can be investigated and shows that it is partially driven by high latitudes values, mainly in Antarctica, as presented in Fig. A1 (see Appendix A). Antarctic isotopic values are not computed correctly due to issues in the conservation of water in the advection scheme at very low humidity content, a fact that was

260 already highlighted in Roche (2013). Improving the conservation in the spectral advection scheme is beyond the scope of the present study. We thus removed these Antarctic values in the following to investigate the isotopic trend without the influence of this region. This results in a better agreement between the GNIP data and iLOVECLIM model (with a correlation coefficient of 0.89 in the model), even if differences are observed with generally lower d-excess value in the model than in the data for low $\delta^2 H_{precipitation}$ (Fig. 4). However, considering the large uncertainties associated with the data, the isotopic values and trends

265 between the model and the data could be closer.

For the d-excess, the range of modelled values can be large for some locations (as already seen in Fig. 1). Thus, we can evaluate the ability of the model to reproduce the d-excess in comparison to the observed data, as presented in Fig. 5. The distribution of most d-excess values is centred around values between 8-18 ‰. Low correlation coefficient is obtained due to outlier d-

270 excess values but statistical significance between the modle and the data is obtained with a p-value of 3e-4 (<0.001). This attests of a good representation of the d-excess in the model (excluding Antarctic values). This is also supported by the modelled d-excess in LMDZ that presents similar values than in iLOVECLIM (Fig. 5). Considering the large uncertainties associated with measurements, the relationship between model and data might vary and get closer to the expected 1:1 line.
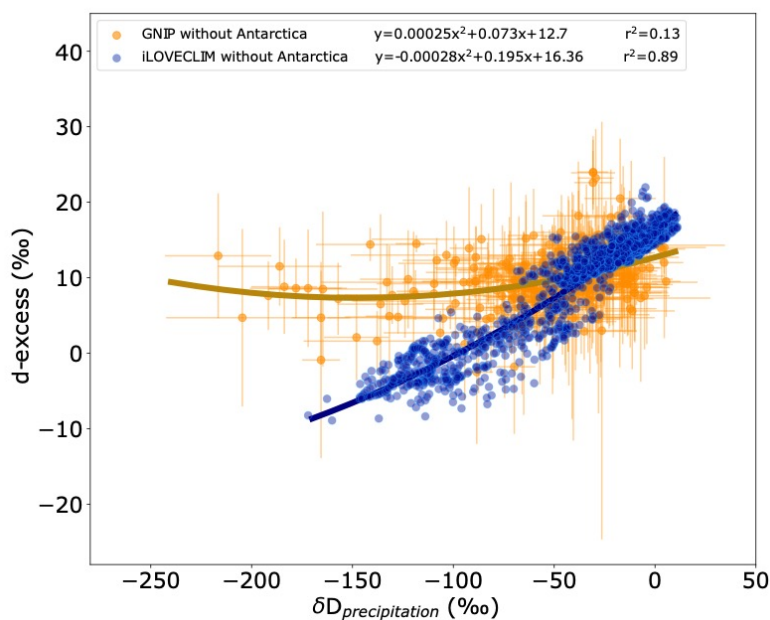
Figure 4: d-excess as a function of δ²H in precipitation without Antarctic values. GNIP data (IAEA, 2006) are presented in orange with the respective error bars (at 2σ) and iLOVECLIM model results are presented in blue. Regression curves are shown for the data (orange) and the model (dark blue).
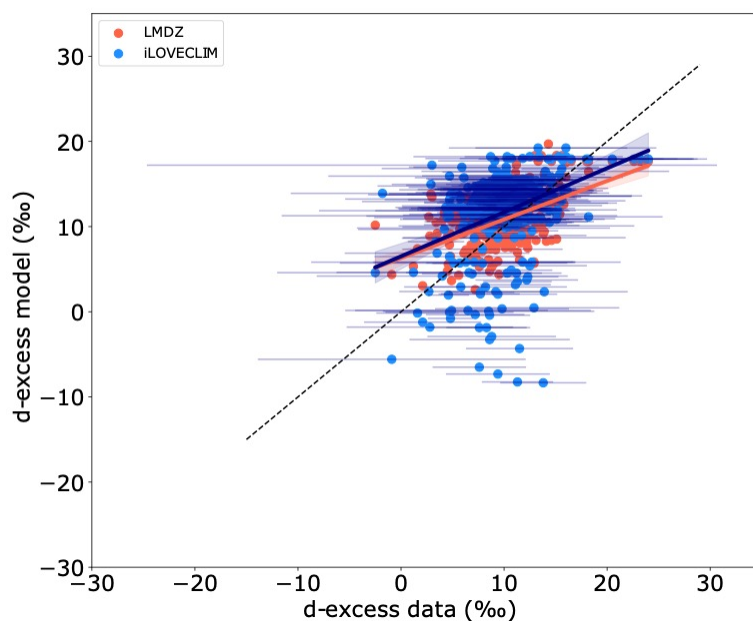
Figure 5: Relationship between the iLOVECLIM modelled d-excess (blue) and the LMDZ4 modelled d-excess (red) versus measurements (GNIP data – IAEA, 2006) without Antarctic values. The errors bars associated with the data are shown at 2σ. The 1:1 line is shown with the black dashed line. Regression lines for iLOVECLIM and LMDZ are in dark blue and red respectively with the confidence bands.

3.1.3 δ^{17}O and ^{17}O-excess distribution

285 We compare iLOVECLIM results with the few observations available for δ^{17}O and ^{17}O-excess. The latitudinal gradient and the global distribution observed for δ^{17}O from the equator to the pole with more depleted values is similar to the one of the δ^{2}H (Fig. 1c). Similarly, the values over land are more depleted than values over the ocean. In comparison to Luz and Barkan (2010) data available over North America, Europe, Asia and Indonesia, iLOVECLIM mostly calculates enriched values of several permil, even if some agreements are observed between the model and the data. These discrepancies can be explained

290 by the fact that the most of the data is punctual and reflect seasonal conditions whereas the model outputs are annual mean δ^{17}O values, and/or due to the uncertainties associated with the measured values. Modelled ^{17}O-excess shares common pattern with δ^{17}O with depleted values over the high latitudes of the Northern Hemisphere and higher values over land (Fig. 1d). The ^{17}O-excess presents values between 0 and 100 permeg over the Atlantic Ocean, that are lower than in the Indian and Pacific oceans. In comparison to the LMDZ model that also has the ^{17}O-excess included (Risi et al., 2013), iLOVECLIM presents

295 higher values for most of the latitudes, due to these high values over the ocean. The latitudinal gradient is also larger than in LMDZ that has relatively homogenous values between 70°S and 90°N. The model seems to reproduce the ^{17}O-excess quite well for some regions with similar values to the observations over North America, Europe and Africa (Fig. 1d). But ^{17}O-excess over the Arabian Sea and northern Canada has probably too negative values. Similarly to d-excess and due to the outlined problem in modelling this region, the ^{17}O-excess modelled over Antarctica present a wide range of values from negative to

300 positive and does not fit with ice core measurements.

Comparison can be done between model and observations for the δ^{17}O$_{precipitation}$ (Fig. 6a) and the ^{17}O-excess (Fig. 6b) to investigate their relationship, even if few data exist. Figure 6a presents the relationship between modelled and measured δ^{17}O$_{precipitation}$ (excluding values in Antarctica). Most of the values modelled in iLOVECLIM are grouped around enriched

305 isotopic values, but the correlation remains low. The p-value is calculated to 0.079 (>0.05), which is slightly higher than the 5 % limit, indicating a close statistical significant between the two parameters. In comparison to LMDZ that is currently the only GCM to include the ^{17}O (Risi et al., 2013), iLOVECLIM results are in good agreement with most of the values between -2 and -5 ‰, leading to similar linear trend between the model and the data (Fig. 6a). One point with negative value of -8.7 ‰ in LMDZ gets closer to the 1:1 line than iLOVECLIM (with -5.8 ‰). However, considering the large confidence intervals for

310 both model results, the modelled δ^{17}O$_{precipitation}$ in iLOVECLIM could be in agreement with the values obtained in LMDZ. The differences between the model results and the data could be related to (1) the uncertainties in measuring this proxy, (2) the fact that most of the data is punctual and reflect seasonal conditions whereas the model outputs are annual mean δ^{17}O values and (3) the low number of measurements to compare with.

Similar comparison can be done for the ^{17}O-excess (Fig. 6b). A wide dispersion of the ^{17}O-excess values (excluding values in

315 Antarctica) is observed, with no clear relationship, mostly due to some highly negative values (up to -116 ‰) in the model,

but statistically significant with a p-value of 0.0023 (<0.05). ^{17}O-excess has also been previously modelled in LMDZ (Risi et al., 2013) and presents similar isotopic composition than the iLOVECLIM results between 10 and 40 ‰ (Fig. 6b). LMDZ modelled ^{17}O-excess is however different than iLOVECLIM and the expected data value (considering the 1:1 line) for extrema values: higher values than data are modelled for depleted values and lower values than data are modelled for enriched values.

320 Considering the confidence interval associated with the model results and the uncertainties listed above on the measurements, our results could get closer to the 1:1 line.
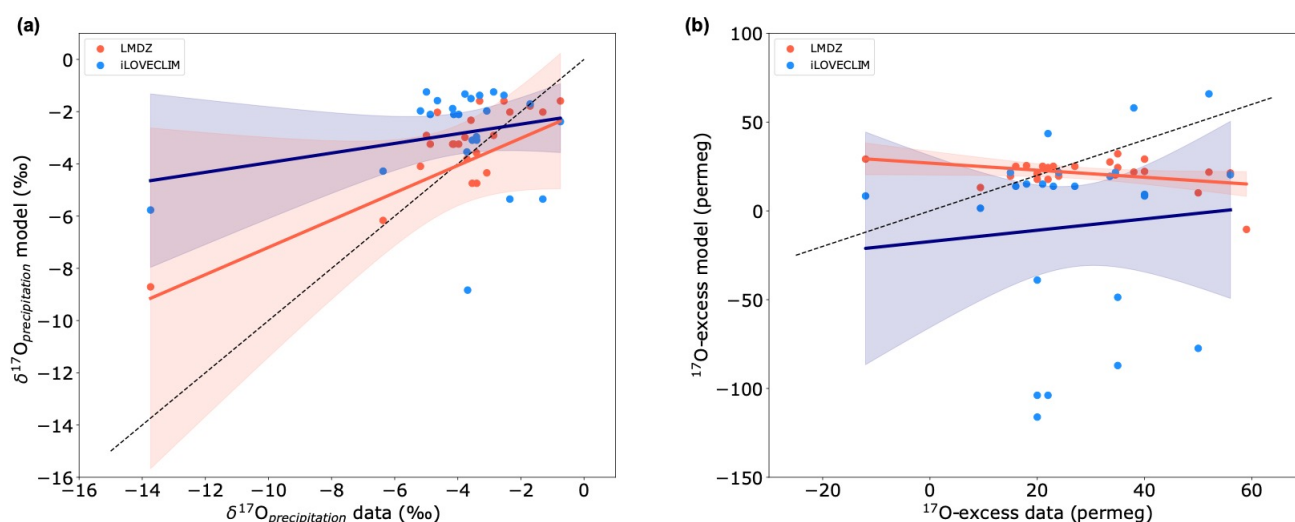
Figure 6: Relationship between the iLOVECLIM modelled isotopic values and data for (a) $\delta^{17}O$ in precipitation and (b) for ^{17}O-
325 **excess, without values in Antarctica. Measurements are from Luz and Barkan (2010) and Tian et al. (2021) for $\delta^{17}O_{precipitation}$ and from Risi et al. (2008); Luz and Barkan (2010); Tian et al. (2021) for ^{17}O-excess. LMDZ model results are also presented for comparison with iLOVECLIM in red (Risi et al., 2013). The regression curves between model and data are presented in dark blue for iLOVECLIM and red for LMDZ with the confidence bands. The 1:1 line are shown with the black dashed lines.**

330 **3.1.4 Seasonal variations**

We compare the seasonal model results to the GNIP monthly data at several locations in South Africa (Pretoria), South America (Belem), eastern Mediterranean (Ankara) and northern Atlantic (Reykjavik) to have a global overview. We extracted the model results at the corresponding locations but due to the coarse resolution of the model, regional biases exist as depicted in previous section. The seasonal evolution of precipitation and isotopic composition in the model is then not expected to perfectly reflect
335 the measurements. We then present the normalized values for both model and GNIP data. There is a good agreement in precipitation at Pretoria and Ankara between the observation and the model that correctly reproduce the seasonal cycle (Fig. 7). For Belem and Reykjavik stations the model shows some differences, namely higher precipitations in September and October at Belem and higher monthly amplitude at Reykjavik. Good correlation is observed for the modelled $\delta^2H_{precipitation}$ in

comparison to observations at Pretoria and Ankara (even if the October value is largely depleted). As for precipitations, the

340   amplitude of $\delta^2H_{precipitation}$ variations is different between the model and the data at Belem and Reykjavik (Fig. 7). But the

overall model behaviour in reproducing seasonal variations of $\delta^2H_{precipitation}$ can be validated based on these observations,

especially when taking into account the uncertainties associated with the data that can be as large as the measurement itself.

The d-excess variations show however larger differences between the model and the observations. The modelled d-excess at

Reykjavik shows a good agreement with the observation, while larger amplitude of the variations is observed at Belem (Fig.

345   7). At Ankara, the modelled d-excess is delayed during summer compared to observations and shows too low values in October.

At Pretoria, even if the $\delta^2H_{precipitation}$ is correctly reproduced in the model, the d-excess presents differences with enriched values

between May and September, whereas the data indicates lower values during this period. However, taking into account the

uncertainties associated with the GNIP data, our model results fit within the range of values obtained for the measurements.
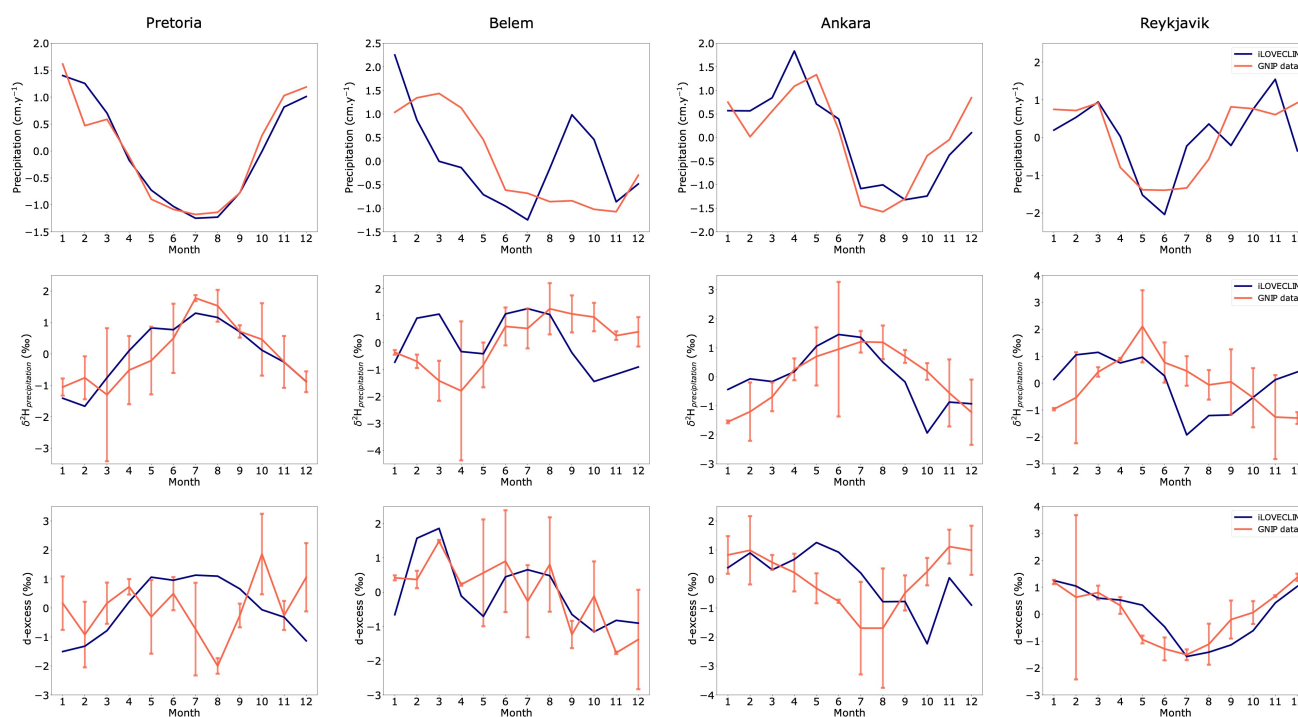
Figure 7: Monthly evolution of precipitation (top row), $\delta^2H_{precipitation}$ (middle row) and d-excess (bottom row) at several stations (different columns for Pretoria, Belem, Ankara and Reykjavik). The red line is the GNIP data measured at the station (IAEA/WMO, 2023) and the blue line is the iLOVECLIM model result at the corresponding location. The GNIP data and model results have been normalized for easier comparison (we subtracted the mean and divided by the standard deviation for each station). The error bars for the GNIP data are also shown at 2σ.

3.2 Oceanic isotopic composition

3.2.1 Surface waters δ^2H and d-excess

360   The hydrogen isotopic composition has also been modelled in the oceanic component for the sea water. We first look at the surface distribution of the isotopes using modelled values for the first oceanic layer at 5 m depth. For quantitative evaluation of the model results, we selected GISS sea water values between 0 and 10 m to be representative of the surface (Schmidt et al., 1999). iLOVECLIM models annual mean surface δ^2H$_{seawater}$ with low values in the Arctic Ocean, that match the few existing data points at high latitudes. The δ^2H$_{seawater}$ in the Atlantic Ocean is also well reproduced in the model with high

365   enriched values close to the tropic and the equator and lower values in the northern and southern part of the ocean, even if the modelled values are slightly different than the observation in the northern Atlantic (Fig. 8a). The Mediterranean Sea presents a good agreement with the observation with high δ^2H$_{seawater}$ values. The δ^2H$_{seawater}$ pattern in the Pacific and Austral oceans is also similar to the observations. However, the western part of the Indian Ocean and Arabian Sea presents lower values of ~10 ‰ in comparison to the GISS data (Fig. 8a). This could be explained by a model bias toward higher precipitations and reduced

370   salinity in this area. The annual mean surface δ^2H$_{seawater}$ modelled in iLOVECLIM can also be compared to other coupled model with isotopes like MPI-ESM (Cauquoin et al., 2020) from the zonal distribution of the isotopic composition. In this case, the δ^2H$_{seawater}$ has been calculated from δ^{18}O$_{seawater}$ and d-excess outputs of MPI-ESM. The overall δ^2H$_{seawater}$ distribution of both models fit in the range of δ^2H$_{seawater}$ observation values at the surface of the ocean (Schmidt et al. 1999), with a mean zonal value close to zero for mid-low latitudes and lower values at higher latitudes (Fig. 9). However, the change in δ^2H$_{seawater}$

375   in iLOVECLIM presents a smaller amplitude from the equator to Greenland than MPI-ESM that shows larger δ^2H$_{seawater}$ decrease up to -27 ‰. This progressive depletion in δ^2H$_{seawater}$ better match the data that also indicate a decrease in δ^2H$_{seawater}$ value between 40 and 90°N (Fig. 9).

The annual mean surface d-excess in the different oceanic basins is also presented in Fig. 8b with the GISS data for comparison.

380   The overall pattern of d-excess is similar to the one of the δ^2H$_{seawater}$ with high positive values in the Arctic Ocean and lower depleted values in the Atlantic, Pacific, Indian and Austral oceans. The modelled d-excess values from -2 to 0 ‰ in the Atlantic and Pacific oceans match the observations, with a small gradient from the high to low latitudes (Fig. 8b). The western part of the Indian Ocean and the Arabian Sea again presents different values than the observations. The model calculates a d-excess of ~2 ‰ in the western Indian ocean whereas the data have smaller values. The modelled d-excess even goes up to 14 ‰ in

385   the Arabian Sea, due to precipitation and humidity effect. Even if a small number of data points exist in the Polar Ocean above 60°N (only few measurements in the Atlantic sector), the model reproduces too high d-excess value in comparison to the observations. These enriched values could be associated to the absence of sea ice in this simulation, that would lead to fractionation during sea ice formation and depletion of the liquid water isotopic composition.
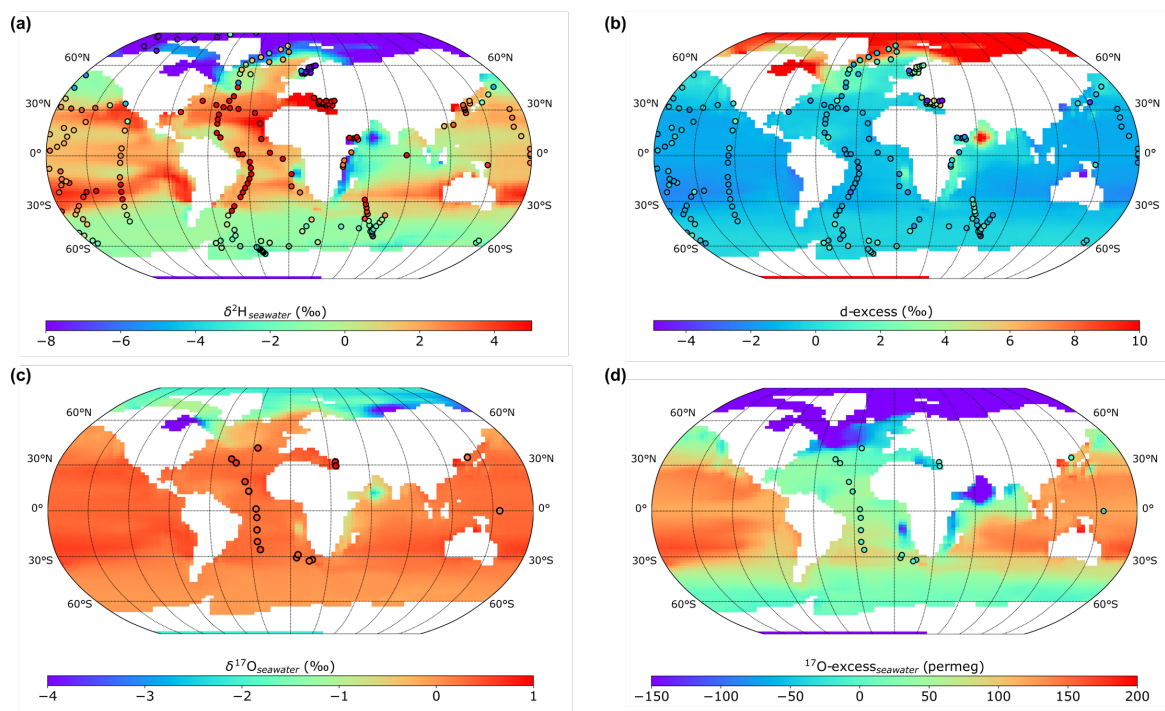
390

Figure 8: Model-data comparison of the annual mean isotopic distribution in the ocean. (a) δ²H of ocean surface water in iLOVECLIM compared to the GISS database (Schmidt et al., 1999). (b) d-excess of ocean surface water in iLOVECLIM compared to the GISS database (Schmidt et al., 1999). (c) δ¹⁷O of ocean surface water in iLOVECLIM compared to Luz and Barkan (2010) data. (d) ¹⁷O-excess of ocean surface water in iLOVECLIM compared to Luz and Barkan (2010) data.

395
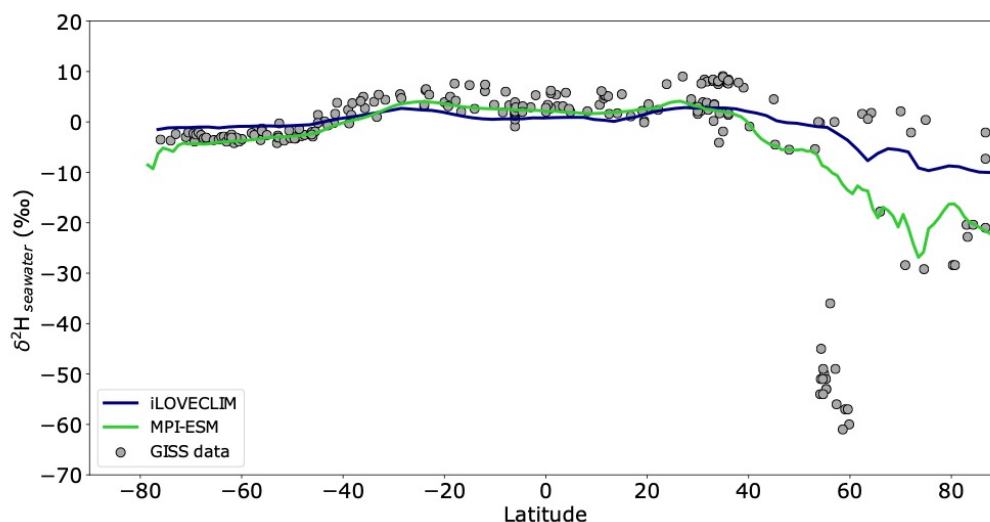
Figure 9: Zonal annual mean δ²H of ocean surface water in iLOVECLIM (blue line) compared to MPI-ESM enabled isotopes model (green line – Cauquoin et al., 2020) and to the GISS data (grey points – Schmidt et al., 1999).

3.2.2 Distribution at depth

The model-data comparison of δ²H and d-excess of sea water can be realized over the entire water column with a cross section in the Atlantic Ocean. We find a general good agreement between the GISS observation and the model from the surface to the bottom with the imprint of the different water masses on the simulated δ²H (Fig. 10a). The strongest δ²H enrichment is observed in the upper Atlantic (above 700 m) between 30°S and 45°N with a maximum around 20°N with 4.2 ‰. There are however some differences in the surface water with δ²H values that are higher by several permil in the observation than in the model. Below 700 m, the North Atlantic deep waters (NADW) have lower δ²H values, between 1.8 and up to 0 ‰ at the bottom of the ocean where they mix with the Antarctic bottom water (AABW) coming from the South with depleted values (Fig. 10a). In the Southern Ocean around 1000 m depth, the Antarctic intermediate waters (AAIW) flow to the north with negative depleted δ²H values. The oceanic d-excess shows less prominent influence of the main water masses. Above 1000 m, the d-excess goes from 40°S to 40°N with depleted negative values (Fig. 10b). Below 1000 m and from 40°S to the north, the NADW d-excess values are higher with a maximum of 2 ‰ around 25°N and 2000 m depth. The comparison with the GISS data shows that the model reproduces the depleted surface values and the enriched d-excess values below 1800 m even if the latitudinal gradient is more pronounced in the model than in the data. The depth interval from 500 to 1800 m presents a disagreement between the modelled d-excess and the observation values that are consistently lower than in the model (Fig. 10b). This is especially the case for high latitudes of the northern hemisphere where the difference between the model and the data can reach 2 to 3 ‰.
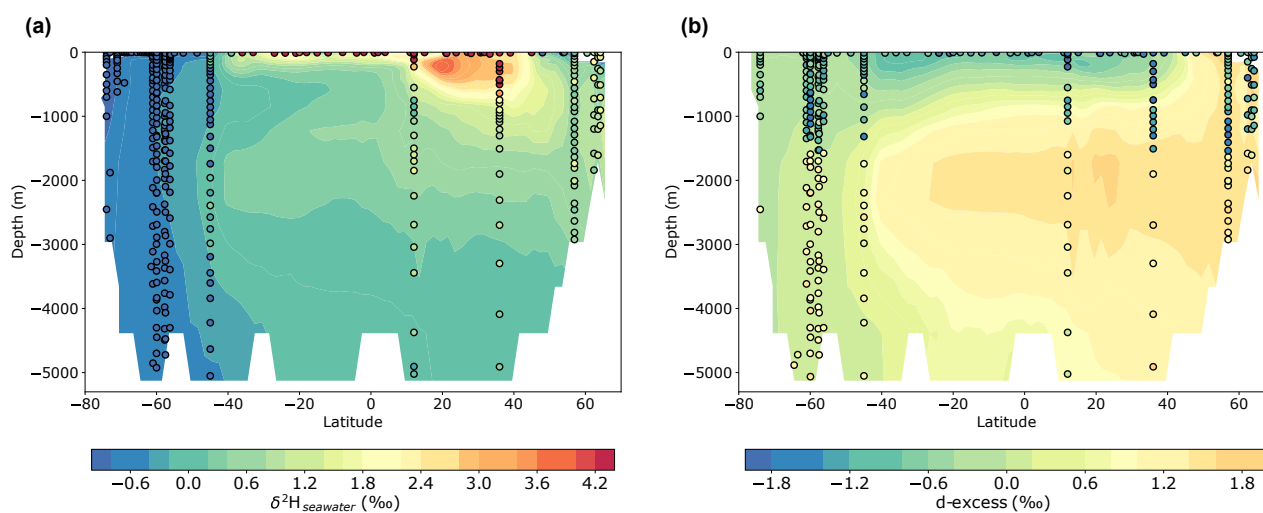
Figure 10: Atlantic zonal mean in iLOVECLIM of (a) δ²H of seawater and (b) d-excess of seawater, compared to GISS database (Schmidt et al., 1999).

3.2.3 δ^{17}O and ^{17}O-excess

δ^{17}O of seawater in iLOVECLIM shows relatively similar close to zero values over the Atlantic, Pacific, Indian and Southern
425 oceans which is consistent with the observations from Luz and Barkan (2010) (Fig. 8c). The amplitude of variation is small
and around 1 ‰. The coast of east Africa and the Arabian sea present lower values, as well as the northern part of the Atlantic
Ocean and the Arctic Sea with negative values up to -4 ‰. As for ^{17}O-excess, modelled values are as well highly depleted in
the entire Arctic Ocean, Arabian Sea, Mediterranean Sea and along the coast of east and west Africa (Fig. 8d). Apart from the
northern part that has negative values similar to the Arctic Ocean, the Atlantic Ocean presents relatively small ^{17}O-excess
430 variations and match the data with values between 0 and 50 permeg. The Pacific and Indian oceans have higher ^{17}O-excess
values up to 200 permeg, which is higher than observations. However, the lack of data does not allow a good model-data
evaluation for this proxy.

Conclusions

In this study, we presented the implementation of the δ^{2}H and δ^{17}O water isotopic composition in the intermediate complexity
435 coupled climate model iLOVECLIM. Based on the existing δ^{18}O water isotopic module and on this new extension, we also
modelled the d-excess and ^{17}O-excess variations to have a general overview of the water isotopes. We evaluated the model
isotopic composition for preindustrial for both the atmosphere and the ocean components based on a long equilibrium
simulation. For the atmospheric part, we found a good agreement between the model and the GNIP data (considering the
intrinsic biases of iLOVECLIM that could lead to local inconsistencies), with the conservation of the latitudinal gradient. The
440 modelled δ^{2}H and δ^{18}O also fit with the global Meteorological Water Line. The d-excess distribution for the atmosphere is also
well reproduced at global scale in the model in comparison to the observations and other GCMs. The isotopic composition of
oxygen and hydrogen over Antarctica present differences of several permil in comparison to the data because of the complexity
of the local processes at play that are simplified in the model. For a better agreement between the model and the data, or at
least more robust comparison between the different isotopic parameters, more measurements are needed and their associated
445 uncertainties need to be reduced, in particular for the δ^{17}O and ^{17}O-excess. For the ocean, we reproduced a good accordance
of the modelled surface δ^{2}H, δ^{17}O and d-excess in comparison to the data, except for some parts of the Arctic region and local
areas in the Indian Ocean. This good agreement is conserved over the entire water column in the Atlantic Ocean, with similar
δ^{2}H values and distribution between the model and the data, influenced by the main water masses.

450 This study opens up several future potential applications. New proxies that depend on the water isotopes can be implemented
in the model, like the leaf wax isotopic composition, in order to quantify the influence of the respective factors (precipitation,
vegetation, humidity…) that control its variations. Paleoclimate simulations during the Holocene, Last Glacial Maximum or
older glacial/interglacial periods are also the next logical step to compare model results against past isotopic composition
records.

Appendix A: d-excess vs δ²H relationship

From the globally available data, a relationship between d-excess and $\delta^2H_{precipitation}$ exists with high d-excess value (~15 ‰) for highly depleted $\delta^2H_{precipitation}$ values (around -400 and 0 ‰), whereas lower d-excess is observed for mean $\delta^2H_{precipitation}$ between -250 and -300 ‰ (Fig. A1). The low $\delta^2H_{precipitation}$ values correspond to high latitudes values (above 60°N and below 60°S), mostly corresponding to Antarctic values, that drive the relationship between d-excess and $\delta^2H_{precipitation}$ (R^2=0.50 when considering all values, R^2=0.10 for values without the high latitudes). Similar relationship between the d-excess and $\delta^2H_{precipitation}$ is observed in the iLOVECLIM model. Highest d-excess values are obtained for low $\delta^2H_{precipitation}$ values (around -200 ‰) and lower d-excess for intermediate $\delta^2H_{precipitation}$ (Fig. A1). The shape of the regression curves is however different between the data and the model because of outlier modelled d-excess values that are too high in the model. These data points mainly correspond to Antarctic values as already observed on Fig. 1. This can be explained by the fact that the model does not correctly estimate the water isotope composition over Antarctica, consequence of the non-conservative behaviour of the advection scheme at very low moisture content and absence of kinetic fractionation coefficient. If we remove all values located at high latitudes (above 60°N and below 60°S), we obtain a good relationship between d-excess and $\delta^2H_{precipitation}$ in the model with a R^2=0.71 (Fig. A1).
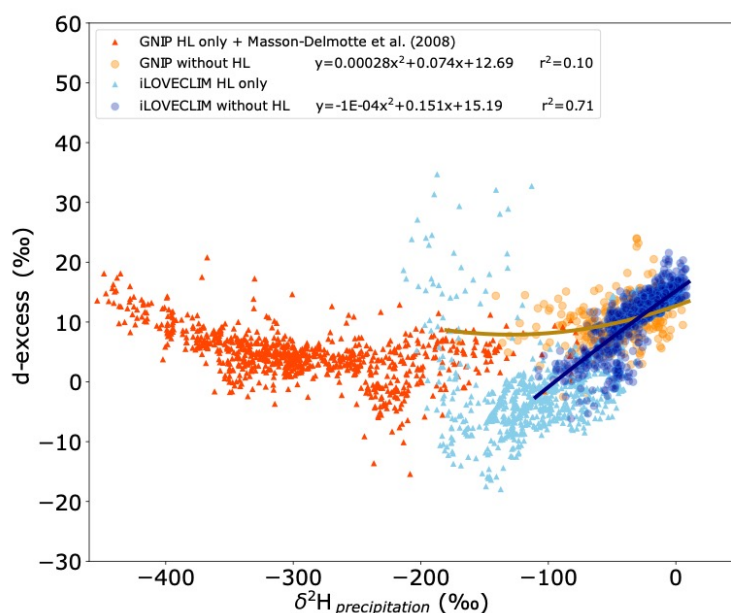
Figure A1: d-excess as a function of δ²H in precipitation. High latitude values (above 60°N and below 60°S) are presented with the red triangles for the GNIP (IAEA, 2006) and Masson-Delmotte et al. (2008) data and with the light blue triangles for iLOVECLIM. Data for other regions are presented with the orange circles for GNIP (IAEA, 2006) and with the dark blue circles for the model. Regression curves for the data and the model, without high latitudes values, are also shown in orange and dark blue.

Author contributions. TE and TC designed the study. DMR realized the model development. TE performed and analysed the simulations with inputs from TC. TE wrote the paper with contributions from all co-authors.

Competing interest. The authors declare that they have no conflict of interest.

480

Code availability. The iLOVECLIM source code and developments are hosted at http://forge.ipsl.jussieu.fr/ludus (IPSL, 2023) but are not publicly available due to copyright restrictions. Access can be granted on demand by request to D.M. Roche (didier.roche@lsce.ipsl.fr) to those who conduct research in collaboration with the iLOVECLIM user group.

485 *Financial support.* This research was supported by the ANR HYDRATE project, grant ANR-21-CE01-0001-01 of the French Agence Nationale de la Recherche.

Acknowledgments. T.C. is supported by CNRS-INSU.

References

490 Barkan, E. and Luz, B.: High precision measurements of $^{17}O/^{16}O$ and ^{18}O /^{16}O ratios in H_2O, Rapid Commun. Mass Sp., 19, 3737–3742, doi:10.1002/rcm.2250, 2005.

Barkan, E. and Luz, B.: Diffusivity fractionations of $H_2{}^{16}O/H_2{}^{17}O$ and $H_2{}^{16}O/H_2{}^{18}O$ in air and their implications for isotope hydrology, Rapid Commun. Mass Spectrom., 21, 2999–3005, doi:10.1002/rcm.3180, 2007.

Berger, A.: Long-term variations of caloric insolation resulting from earths orbital elements, Quaternary Res., 9, 139–167,
495 doi:10.1016/0033-5894(78)90064-9, 1978.

Brutsaert, W. A.: Theory for local evaporation (or heat transfer) from rough and smooth surfaces at ground level, Water Resour. Res., 11, 543–550, https://doi.org/10.1029/WR011i004p00543, 1975.

Caley, T., Kim, J.-H., Malaizé, B., Giraudeau, J., Laepple, T., Caillon, N., Charlier, K., Rebaubier, H., Rossignol, L., Castañeda, I. S., Schouten, S., and Sinninghe Damsté, J. S.: High-latitude obliquity as a dominant forcing in the Agulhas
500 current system, Clim. Past, 7, 1285–1296, doi:10.5194/cp-7-1285-2011, 2011.

Caley, T. and Roche, D. M.: $\delta^{18}O$ water isotope in the iLOVECLIM model (version 1.0) – Part 3: A palaeo-perspective based on present-day data–model comparison for oxygen stable isotopes in carbonates, Geosci. Model Dev., 6, 1505–1516, https://doi.org/10.5194/gmd-6-1505-2013, 2013.

Caley, T., and Roche, D. M.: Modeling water isotopologues during the last glacial: Implications for quantitative paleosalinity
505 reconstruction, Paleoceanography, 30(6), 739-750, https://doi.org/10.1002/2014PA002720, 2015.

Cappa, C. D., Hendricks, M. B., DePaolo, D. J., and Cohen, R. C.: Isotopic fractionation of water during evaporation, J. Geophys. Res., 108, 4525, doi:10.1029/2003JD003597, 2003.

Cauquoin, A., Werner, M., and Lohmann, G.: Water isotopes – climate relationships for the mid-Holocene and preindustrial period simulated with an isotope-enabled version of MPI-ESM, Clim. Past, 15, 1913–1937, https://doi.org/10.5194/cp-15-1913-2019, 2019.

Cauquoin, A., Werner, M., Lohmann, G.: MPI-ESM-wiso simulations data for preindustrial and mid-Holocene conditions, PANGAEA, https://doi.org/10.1594/PANGAEA.912258, 2020.

Collins, J. A., Schefuss, E., Mulitza, S., Prange, M., Werner, M., Tharammal, T., Paul, A., and Wefer, G.: Estimating the hydrogen isotopic composition of past precipitation using leaf-waxes from western Africa, Quaternary Sci. Rev., 65, 88–101, https://doi.org/10.1016/j.quascirev.2013.01.007, 2013.

Craig, H.: Isotopic Variation in Meteoric Waters, Science, 133, 1702–1703, doi:10.1126/science.133.3465.1702, 1961.

Craig, H. and Gordon, L.: Deuterium and oxygen 18 variations in the ocean and the marine atmosphere, Consiglio Nazionale delle Ricerche, Laboratorio di Geologia Nuclerne, Pisa, 9–130, 1965.

Dansgaard, W.: Stable isotopes in precipitation. Tellus, 16(4) :436–468, https://doi.org/10.3402/tellusa.v16i4.8993, 1964.

Goosse, H., Brovkin, V., Fichefet, T., Haarsma, R., Huybrechts, P., Jongma, J., Mouchet, A., Selten, F., Barriat, P.-Y., Campin, J.- M., Deleersnijder, E., Driesschaert, E., Goelzer, H., Janssens, I., Loutre, M.-F., Morales Maqueda, M. A., Opsteegh, T., Mathieu, P.-P., Munhoven, G., Pettersson, E. J., Renssen, H., Roche, D. M., Schaeffer, M., Tartinville, B., Timmermann, A., and Weber, S. L.: Description of the Earth system model of intermediate complexity LOVECLIM version 1.2, Geosci. Model Dev., 3, 603–633, doi:10.5194/gmd-3-603-2010, 2010.

Hou, J., D'Andrea, W. J., and Huang, Y.: Can sedimentary leaf waxes record D / H ratios of continental precipitation? Field, model, and experimental assessments, Geochim. Cosmochim. Ac., 72, 3503–3517, https://doi.org/10.1016/j.gca.2008.04.030, 2008.

IAEA: Isotope Hydrology Information System, The ISOHIS Database, available at: https://www.iaea.org (last access: 8 March 2012), 2006.

IAEA/WMO: Global Network of Isotopes in Precipitation. The GNIP Database. Accessible at: https://nucleus.iaea.org/wiser (last access: 4 May 2023), 2023.

IPSL: LUDUS Framework, https://forge.ipsl.jussieu.fr/ludus, last access: 17 April 2023.

Johnsen, S. J., Dansgaard, W., Clausen, H. B., and Langway, C. C.: Oxygen isotope profiles through the Antarctic and Greenland ice sheets, Nature, 235, 429–434, https://doi.org/10.1038/235429a0, 1972.

Jouzel, J., Vimeux, F., Caillon, N., Delaygue, G., Hoffmann, G., Masson-Delmotte, V., and Parrenin, F.: Magnitude of isotope/temperature scaling for interpretation of central Antarctic ice cores, J. Geophys. Res.-Atmos., 108, D124361, doi:10.1029/2002JD002677, 2003.

Kahmen, A., Schefuß, E., and Sachse, D.: Leaf water deuterium enrichment shapes leaf wax n-alkane δD values of angiosperm plants I: Experimental evidence and mechanistic insights, Geochim. Cosmochim. Ac., 111, 39–49, https://doi.org/10.1016/j.gca.2012.09.003, 2013a.

Kahmen, A., Hoffmann, B., Schefuß, E., Arndt, S. K., Cernusak, L. A., West, J. B., and Sachse, D.: Leaf water deuterium enrichment shapes leaf wax n-alkane δD values of angiosperm plants II: observational evidence and global implications, Geochim. Cosmochim. Ac., 111, 50–63, https://doi.org/10.1016/j.gca.2012.09.004, 2013b.

Kuechler, R. R., Schefuß, E., Beckmann, B., Dupont, L., and Wefer, G.: NW African hydrology and vegetation during the 545 Last Glacial cycle reflected in plant-wax-specific hydrogen and carbon isotopes, Quaternary Sci. Rev., 82, 56–67, https://doi.org/10.1016/j.quascirev.2013.10.013, 2013.

Kurita, N., Noone, D., Risi, C., Schmidt, G. A., Yamada, H., and Yoneyama, K.: Intraseasonal isotopic variation associated with the Madden–Julian Oscillation, J. Geophys. Res.-Atmos., 116, D24101, doi:10.1029/2010JD015209, 2011.

Landais, A., Barkan, E., and Luz, B: The triple isotopic composition of oxygen in leaf water, Geochim. Cosmochim. Ac., 70, 550 4105– 4115, https://doi.org/10.1016/j.gca.2006.06.1545, 2006.

Landais, A., Barkan, E., and Luz, B.: Record of $\delta^{18}O$ and ^{17}O-excess in ice from Vostok Antarctica during the last 150000 years, Geophys. Res. Lett., 35, L02709, doi:10.1029/2007GL032096, 2008.

Landais, A., Risi, C., Bony, S., Vimeux, F., Descroix, L., Falourd, S., and Bouygues, A.: Combined measurements of ^{17}O-excess and d-excess in African monsoon precipitation: implications for evaluating convective parameterizations, Earth 555 Planet. Sci. Lett., 298, 104–112, https://doi.org/10.1016/j.epsl.2010.07.033, 2010.

Landais, A., Steen-Larsen, H.-C., Guillevic, M., Masson-Delmotte, V., Vinther, B., and Winkler, R.: Triple isotopic composition of oxygen in surface snow and water vapor at NEEM (Greenland), Geochim. Cosmochim. Ac., 77, 304–316, https://doi.org/10.1016/j.gca.2011.11.022, 2012.

Landais, A., Stenni, B., Masson-Delmotte, V., Jouzel, J., Cauquoin, A., Fourré, E., Minster, B., Selmo, E., Extier, T., Werner, 560 M., Vimeux, F., Uemura, R., Crotti, I., Grisart, A.: Interglacial Antarctic–Southern Ocean climate decoupling due to moisture source area shifts. Nat. Geosci. 14, 918–923, https://doi.org/10.1038/s41561-021-00856-4, 2021.

Leduc, G., Sachs, J. P., Kawka, O. E., and Schneider, R. R.: Holocene changes in eastern equatorial Atlantic salinity as estimated by water isotopologues, Earth Planet. Sc. Lett., 362, 151– 162, https://doi.org/10.1016/j.epsl.2012.12.003, 2013.

Lee, J.-E., Fung, I., DePaolo, D. J., and Henning, C. C.: Analysis of the global distribution of water isotopes using the NCAR 565 atmospheric general circulation model, J. Geophys. Res., 112, D16306, doi:10.1029/2006JD007657, 2007.

LeGrande, A. N. and Schmidt, G. A.: Global gridded data set of the oxygen isotopic composition in seawater, Geophys. Res. Lett., 33, L12604, doi:10.1029/2006GL026011, 2006.

LeGrande, A. N. and Schmidt, G. A.: Water isotopologues as a quantitative paleosalinity proxy, Paleoceanography, 26, PA3225, https://doi.org/10.1029/2010pa002043, 2011.

570 Lewis, S. C., LeGrande, A. N., Kelley, M., and Schmidt, G. A.: Modeling insights into deuterium excess as an indicator of water vapor source conditions, J. Geophys. Res., 118, 243–262, doi:10.1029/2012JD017804, 2013.

Lorius, C., Merlivat, L., Jouzel, J., and Pourchet, M.: A 30,000-yr isotope climatic record from Antarctic ice, Nature, 280, 644–648, https://doi.org/10.1038/280644a0, 1979.

Luz, B. and Barkan, E.: The isotopic ratios $^{17}O/^{16}O$ and $^{18}O/^{16}O$ in molecular oxygen and their significance in bio-geochemistry, Geochim. Cosmochim. Acta., 69, 1099–1110, https://doi.org/10.1016/j.gca.2004.09.001, 2005.

Luz, B. and Barkan, E.: Variations of $^{17}O/^{16}O$ and $^{18}O/^{16}O$ in meteoric waters, Geochim. Cosmochim. Ac., 74, 6276–6286, doi:10.1016/j.gca.2010.08.016, 2010.

Majoube, M.: Fractionnement en oxygène 18 et deutérium entre l'eau et sa vapeur, J. Chim. Phys., 68, 1423–1436, https://doi.org/10.1051/jcp/1971681423, 1971a.

Majoube, M.: Fractionnement en 18O entre la glace et la vapeur d'eau, J. Chim. Phys., 68, 625–636, https://doi.org/10.1051/jcp/1971680625, 1971b.

Masson-Delmotte, V., Jouzel, J., Landais, A., Stievenard, M., Johnsen, S. J., White, J. W. C., Sveinbjornsdottir, A., and Fuhrer, K.: Deuterium excess reveals millennial and orbital scale fluctuations of Greenland moisture origin, Science, 309, 118–121, https://doi.org/10.1126/science.1108575, 2005.

Masson-Delmotte, V., Hou, S., Ekaykin, A., Jouzel, J., Aristarain, A. J., Bernardo, R. T., Bromwich, D., Cattani, O., Delmotte, M., Falourd, S., Frezzotti, M., Gallee, H., Genoni, L., Isaksson, E., Landais, A., Helsen, M. M., Hoffmann, G., Lopez, J., Morgan, V., Motoyama, H., Noone, D., Oerter, H., Petit, J.-R., Royer, A., Uemura, R., Schmidt, G. A., Schlosser, E., Simoes, J. C., Steig, E. J., Stenni, B., Stievenard, M., van den Broeke, M. R., van de Wal, R. S. W., van de Berg, W. J., Vimeux, F., and White, J. W. C.: Database of Antarctic snow isotopic composition, doi:10.1594/PANGAEA.681697, 2008.

Mathieu, R. and Bariac, T.: A numerical model for the simulation of stable isotope profiles in drying soils, J. Geophys. Res., 101, 12685–12696, https://doi.org/10.1029/96JD00223, 1996.

Merlivat, L. and Nief, G.: Fractionnement isotopique lors des changements d'état solide-vapeur et liquide-vapeur de l'eau à des températures inférieures à 0°C, Tellus, 19, 122–127, https://doi.org/10.1051/jcp/1971681423, 1967.

Merlivat, L.: The dependence of bulk evaporation coefficients on Air-Water interfacial conditions as determined by the isotopic method, J. Geophys. Res., 83, 2977–2980, https://doi.org/10.1029/JC083iC06p02977, 1978.

Merlivat, L. and Jouzel, J.: Global Climatic Interpretation of the Deuterium-Oxygen 18 Relationship for Precipitation, J. Geophys. Res., 84, 5029–5033, http://dx.doi.org/10.1029/JC084iC08p05029, 1979.

Risi, C., Bony, S., Vimeux, F., Descroix, L., Ibrahim, B., Lebreton, E., Mamadou, I., and Sultan, B.: What controls the isotopic composition of the African monsoon precipitation? Insights from event-based precipitation collected during the 2006 AMMA campaign, Geophys. Res. Lett., 35, doi:10.1029/2008GL035920, 2008.

Risi, C., Landais, A., Bony, S., Jouzel, J., Masson-Delmotte, V., and Vimeux, F.: Understanding the ^{17}O excess glacial-interglacial variations in Vostok precipitation, J. Geophys. Res.-Atmos., 115, doi:10.1029/2008jd011535, 2010.

Risi, C., Noone, D., Worden, J., Frankenberg, C., Stiller, G., Kiefer, M., Funke, B., Walker, K., Bernath, P., Schneider, M., Wunch, D., Sherlock, V., Deutscher, N., Griffith, D., Wennberg, P.O., Strong, K., Smale, D., Mahieu, E., Barthlott, S., Hase, F., García, O., Notholt, J., Wameke, T., Toon, G., Sayres, D., Bony, S., Lee, J., Brown, D., Uemura, R., and Sturm, C.: Process-evaluation of tropospheric humidity simulated by general circulation models using water vapor isotopologues: 1. Comparison between models and observations, J. Geophys. Res., 117, D05303, doi:10.1029/2011JD016621, 2012.

Risi, C., Landais, A., Winkler, R., and Vimeux, F.: Can we determine what controls the spatio-temporal distribution of d-excess and 17O-excess in precipitation using the LMDZ general circulation model?, Clim. Past, 9, 2173–2193, doi:10.5194/cp-9-2173-2013, 2013.

Roche, D. M.: δ^{18}O water isotope in the iLOVECLIM model (version 1.0) – Part 1: Implementation and verification, Geosci. Model Dev., 6, 1481–1491, doi:10.5194/gmd-6-1481-2013, 2013.

Roche, D. M. and Caley, T.: δ^{18}O water isotope in the iLOVECLIM model (version 1.0) – Part 2: Evaluation of model results against observed δ^{18}O in water samples, Geosci. Model Dev., 6, 1493–1504, https://doi.org/10.5194/gmd-6-1493-2013, 2013.

Rohling, E. J.: Progress in paleosalinity: Overview and presentation of a new approach, Paleoceanography, 22, 1–9, https://doi.org/10.1029/2007PA001437, 2007.

Sachse, D., Billault, I., Bowen, G. J., Chikaraishi, Y., Dawson, T. E., Feakins, S. J., Freeman, K. H., Magill, C. R., McInerney, F. A., van der Meer, M. T. J., Polissar, P., Robins, R. J., Sachs, J. P., Schmidt, H.-L., Sessions, A. L., White, J. W. C., West, J. B., and Kahmen, A.: Molecular paleohydrology: interpreting the hydrogen isotopic composition of lipid biomarkers from photosynthetic organisms, Annu. Rev. Earth Planet. Sci., 40, 221–249, https://doi.org/10.1146/annurev-earth-042711-105535, 2012.

Schefuß, E., Schouten, S., and Schneider, R. R.: Climatic controls on central African hydrology during the past 20000 years, Nature, 437, 1003–1006, https://doi.org/10.1038/nature03945, 2005.

Schmidt, G. A., Bigg, G. R., and Rohling, E. J.: Global seawater oxygen-18 database, available at: https://data.giss.nasa.gov/o18data/ (last access: 3 May 2023), 1999.

Schmidt, G. A., LeGrande, A. N., and Hoffmann, G.: Water isotope expressions of intrinsic and forced variability in a coupled ocean-atmosphere model, J. Geophys. Res., 112, D10103, doi:10.1029/2006JD007781, 2007.

Steiger, N. J., Steig, E. J., Dee, S. G., Roe, G. H., and Hakim, G. J.: Climate reconstruction using data assimilation of water isotope ratios from ice cores, J. Geophys. Res.-Atmos., 122, 1545–1568, https://doi.org/10.1002/2016JD026011, 2017.

Steiger, N.: Historical climate model output of ECHAM5-wiso from 1871-2011 at T106 resolution [data set], https://doi.org/10.5281/zenodo.1249604, 2018.

Stenni, B., Masson-Delmotte, V., Johnsen, S., Jouzel, J., Longinelli, A., Monnin, E., Röthlisberger, R., and Selmo, E.: An oceanic cold reversal during the last deglaciation, Science, 293, 2074–2077, https://doi.org/10.1126/science.1059702, 2001.

Tian, C., Du, K., Wang, L., Zhang, X., Li, F., Jiao, W., Beysens, D., Kaseke, K.F., Medici, M.G.: Stable isotope composition of dew measured from 2014 to 2018 in Namibia, France, and the United States, PANGAEA, https://doi.org/10.1594/PANGAEA.934127, 2021.

Uemura, R., Barkan, E., Abe, O., and Luz, B.: Triple isotope composition of oxygen in atmospheric water vapor, Geophys. Res. Lett., 37, L04402, doi:10.1029/2009gl041960, 2010.

640 Van Breukelen, M. R., Vonhof, H. B., Hellstrom, J. C., Wester, W. C. G., and Kroon, D.: Fossil dripwater in stalagmites reveals Holocene temperature and rainfall variation in Amazonia, Earth Planet. Sc. Lett., 275, 54–60, https://doi.org/10.1016/j.epsl.2008.07.060, 2008.

Vimeux, F., Cuffey, K., and Jouzel, J.: New insights into Southern Hemisphere temperature changes from Vostok ice cores using deuterium excess correction over the last 420 000 years, Earth Planet. Sc. Lett., 203, 829–843,
645 https://doi.org/10.1016/S0012-821X(02)00950-0, 2002.

Vimeux, F., Gallaire, R., Bony, S., Hoffmann, G., and Chiang, J. C. H.: What are the climate controls on δD in precipitation in the Zongo Valley (Bolivia)? Implications for the Illimani ice core interpretation, Earth Planet. Sc. Lett., 240, 205–220, https://doi.org/10.1016/j.epsl.2005.09.031, 2005.

Vonhof, H. B., van Breukelen, M. R., Postma, O., Rowe, P. J., Atkinson, T. C., and Kroon, D.: A continuous-flow crushing
650 device for on-line δ^2H analysis of fluid inclusion water in speleothems, Rapid Commun. Mass Sp., 20, 2553–2558, https://doi.org/10.1002/rcm.2618, 2006.

Werner, M., Langebroek, P. M., Carlsen, T., Herold, M., and Lohmann, G.: Stable water isotopes in the ECHAM5 general circulation model: toward high-resolution isotope modeling on a global scale, J. Geophys. Res., 116, D15109, doi:10.1029/2011JD015681, 2011.

655 Werner, M., Haese, B., Xu, X., Zhang, X., Butzin, M., and Lohmann, G.: Glacial–interglacial changes in $H_2^{18}O$, HDO and deuterium excess – results from the fully coupled ECHAM5/MPI-OM Earth system model, Geosci. Model Dev., 9, 647–670, https://doi.org/10.5194/gmd-9-647-2016, 2016.

Winkler, R., Landais, A., Sodemann, H., Dümbgen, L., Prié, F., Masson-Delmotte, V., Stenni, B., and Jouzel, J.: Deglaciation records of ^{17}O-excess in East Antarctica: reliable reconstruction of oceanic normalized relative humidity from coastal sites,
660 Clim. Past, 8, 1–16, doi:10.5194/cp-8-1-2012, 2012.